Article:
Lockhart, J, Blitz, MA, Heard, DE et al. (2 more authors) (2013) Mechanism of the reaction of OH with alkynes in the presence of oxygen. Journal of Physical Chemistry A, 117 (26). 5407 - 5418. ISSN 1089-5639

https://doi.org/10.1021/jp404233b

Kinetic study of the OH + glyoxal reaction: Experimental evidence and quantification of direct OH recycling

James Lockhart[1], Mark Blitz[1,2], Dwayne Heard[1,2], Paul Seakins*[1,2] and Robin Shannon[1]
[1]*University of Leeds, Leeds, LS2 9JT, UK*
[2]*National Centre for Atmospheric Science, University of Leeds, Leeds, LS2 9JT, UK*

Abstract

The kinetics of the OH + glyoxal, $(HCO)_2$, reaction have been studied in N_2 and N_2/O_2 bath gas from 5 – 80 Torr total pressure and 212 – 295 K, by monitoring the OH decay via laser induced fluorescence (LIF) in excess $(HCO)_2$. The following rate coefficients, $k_{OH + (HCO)2}$ = (9.7 ± 1.2), (12.2 ± 1.6) and (15.4 ± 2.0) × 10^{-12} cm^3 $molecule^{-1}$ s^{-1} (where errors represent a combination of statistical errors at the 2σ level and estimates of systematic errors) were measured in nitrogen at temperatures of 295, 250 and 212 K, respectively. Rate coefficient measurements were observed to be independent of total pressure, but decreased following addition of O_2 to the reaction cell, consistent with direct OH recycling. OH yields, Φ_{OH}, for this reaction were quantified experimentally for the first time as a function of total pressure, temperature and O_2 concentration. The experimental results have been parameterised using a chemical scheme where a fraction of the HC(O)CO population promptly dissociates to HCO + CO, the remaining HC(O)CO either dissociates thermally or reacts with O_2 to give CO_2, CO and regenerate OH. A maximum Φ_{OH} of (0.38 ± 0.02) was observed at 212 K, independent of total pressure, suggesting that ~60 % of the HC(O)CO population promptly dissociates upon formation. Qualitatively similar behaviour is observed at 250 K, with a maximum Φ_{OH} of (0.31 ± 0.03); at 295 K the maximum Φ_{OH} decreased further to (0.29 ± 0.03). From the parameterization an OH yield of Φ_{OH} = 0.19 is calculated for 295 K and 1 atm of air. It is shown that the proposed mechanism is consistent with previous chamber studies. Whilst the fits are robust, experimental evidence suggests that the system is influenced by chemical activation and cannot be fully described by thermal rate coefficients. The atmospheric implications of the measurements are briefly discussed.

Keywords: Chemical Activation, Reaction Kinetics, Glyoxal Oxidation, RO_2 isomerizations

Introduction

Glyoxal, $(HCO)_2$, is an important atmospheric trace gas, produced in high yields following oxidation of both biogenic VOCs such as isoprene,[1] and anthropogenic hydrocarbons such as benzene[2-4] and acetylene.[5-7] $(HCO)_2$ is the simplest α-dicarbonyl and its atmospheric significance stems from its role in aerosol formation,[8-10] and use as a marker of biogenic emission.[11,12] In addition, $(HCO)_2$ photochemistry is a recognised source of HOx (OH and HO_2) radicals in the troposphere.[13-15] $(HCO)_2$ is removed from the troposphere within a few hours, during daylight its atmospheric lifetime is largely determined by the rates of photolysis and reaction with OH:[13,16-18]

$$(HCO)_2 + h\nu \rightarrow 2HCO \text{ or } HCHO + CO \qquad \text{(R1)}$$

$$(HCO)_2 + OH \rightarrow HC(O)CO + H_2O \qquad \text{(R2)}$$

Several experimental and theoretical studies have been conducted that focus on $(HCO)_2$ oxidation. Niki et al.[19] studied the Cl atom initiated oxidation of $(HCO)_2$ in chamber experiments using various N_2-O_2 bath gas mixtures at 700 Torr and 298 K, with FTIR product detection.[19] These authors were the first to consider the subsequent fate of the HC(O)CO radical and concluded that under atmospheric conditions, HC(O)CO chemistry is governed by a competition between unimolecular dissociation and bimolecular reaction with O_2, the latter including both a direct abstraction pathway (R4a) and an association channel (R4b):

$$HC(O)CO \rightarrow HCO + CO \qquad \text{(R3)}$$

$$HC(O)CO + O_2 \rightarrow 2CO + HO_2 \qquad \text{(R4a)}$$

$$HC(O)CO + O_2 \rightarrow HC(O)C(O)O_2 \qquad \text{(R4b)}$$

Stable product analysis confirmed the formation of both CO and CO_2 in the presence of O_2.[19] While CO production is consistent with reactions 3 and 4, CO_2 formation is not; Niki et al. suggested that reaction of $HC(O)C(O)O_2$ with HO_2 (R5) was potentially responsible, with co-production of radical species, HCO (rapidly converted to HO_2) and OH:

$$HC(O)C(O)O_2 + HO_2 \rightarrow HCO + CO_2 + OH + O_2 \qquad (R5)$$

Orlando and Tyndall[20] generated the HC(O)CO radical via both Cl atom and OH initiated oxidation of $(HCO)_2$ in an environmental chamber/FTIR system at 700 Torr between 224-314 K. Their study reported CO and CO_2 production associated with HC(O)CO chemistry, in agreement with Niki et al., and adopting the same mechanism, showed the $[CO]/[CO_2]$ product ratio scales linearly with the inverse O_2 partial pressure, with a gradient equal to k_3/k_{4b}. The analysis by Orlando and Tyndall provides evidence of a significant barrier to unimolecular decomposition of the HC(O)CO radical (~ 32 kJ mol^{-1}), consequently k_3 exhibits a significant temperature dependence. Conversely, k_{4b} is relatively insensitive to temperature, such that unimolecular decomposition fails to compete with bimolecular reaction with O_2 at 224 K.

More recently, Feierabend et al.[17] studied the kinetics of OH + $(HCO)_2$, monitoring OH directly via LIF, and reported the rate of OH decay to slow following addition of O_2 to the reaction cell. These observations confirm OH production occurs via a primary reaction and not from secondary chemistry as proposed in chamber studies, and are consistent with recent calculations by da Silva[21] which identified a novel chemically activated HC(O)CO + O_2 channel that proceeds directly to CO_2, CO and OH (Reaction 6, Figure 1), and suggested this channel is competitive with unimolecular dissociation.

$$HC(O)CO + O_2 \rightarrow CO_2 + CO + OH \qquad (R6)$$

Setokuchi[22] extended the analysis in a theoretical study that considered the energy partitioned in the nascent HC(O)CO radical and concluded that under atmospheric conditions, 91% of the HC(O)CO promptly decomposes on formation.

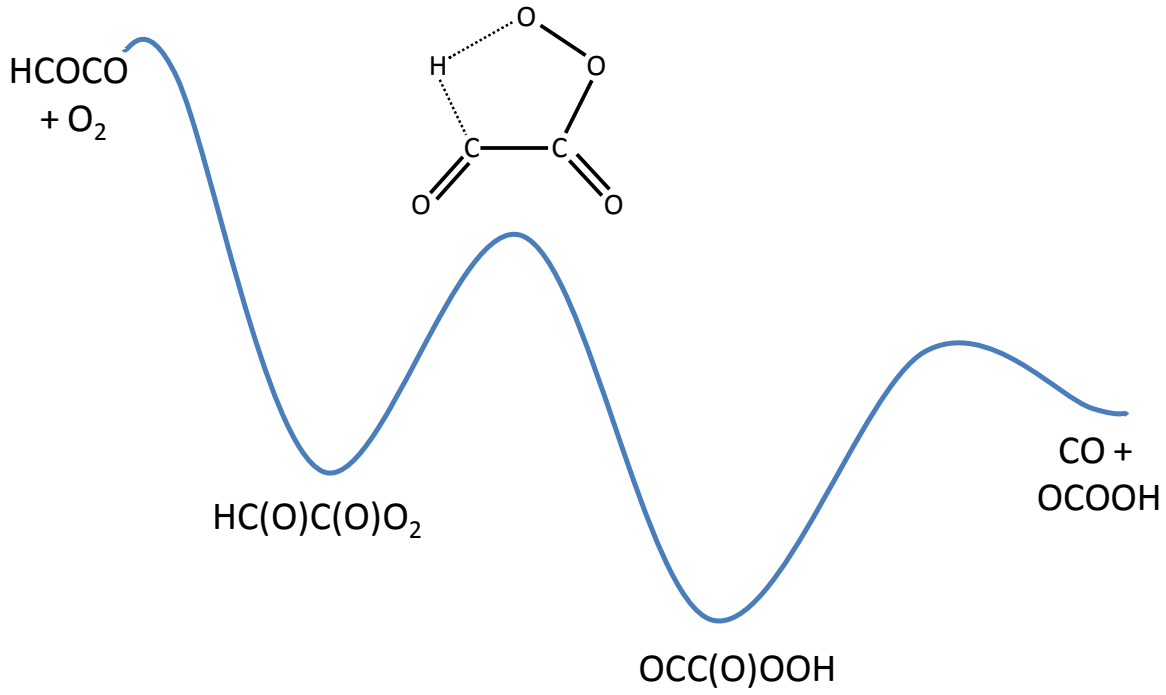

Figure 1. Schematic of the potential energy surface showing the initial addition of O_2 followed by an internal H transfer and then elimination of CO. The OCOOH rapidly dissociates to OH and CO_2. Adapted from da Silva.[21]

Both proposed mechanisms for the fate of HC(O)CO following reaction with O_2 are effectively HOx neutral, although the Niki et al. mechanism requires a radical-radical reaction to regenerate OH, whereas the mechanism proposed by da Silva directly regenerates OH, and therefore occurs on a faster timescale which is independent of the initial radical (Cl/OH) concentration.

In recent decades, field measurements of OH and HO_2 radicals in unpolluted atmospheres have highlighted a major failure of the current scientific understanding of HOx chemistry in regions characterised by both low concentrations of nitrogen oxides, and high concentrations of isoprene and other biogenic volatile organics.[23-26] Measured OH concentrations in pristine environments are consistently higher than those predicted by atmospheric chemical models, and the discrepancy between the observed and modelled OH concentration correlates with the presence of isoprene. Recent field measurements of $(HCO)_2$ made over the rainforest canopy in Borneo have reported peak concentrations of ~ 1.6 ppb, significantly higher than measurements made during other field campaigns in remote forested regions.[27] Furthermore, model analysis has shown $(HCO)_2$ concentrations ($(HCO)_2$ is a known isoprene oxidation product) of this magnitude are consistent with the higher than expected OH concentrations reported in the same region.[27] Given the current uncertainty in isoprene oxidation mechanisms[28-30] and HOx measurements,[31,32] and the link between glyoxal and biogenic emissions, there is a clear need to fully understand OH/glyoxal/O_2 chemistry.

In this study we provide evidence that OH is produced directly following the HC(O)CO + O_2 association reaction, and that the HC(O)CO radical produced following the OH + $(HCO)_2$ reaction either dissociates (both thermally and promptly via a chemically activated process), or reacts with O_2 to regenerate OH. We report experimental OH yield, Φ_{OH}, measurements for the OH + $(HCO)_2/O_2$ reaction as a function of pressure, temperature and O_2 concentration for the first time.

Experimental

This work has been carried out in a conventional slow-flow, laser flash photolysis, laser induced fluorescence (LIF) apparatus that has been used in several previous publications.[5,33-37] The flows of the radical precursor, glyoxal and bath gas (N_2 and/or O_2) were regulated via calibrated mass flow controllers, mixed and flowed into a stainless steel 6-way cross reactor. The reactor was welded into a metal bath, such that only the end flanges of the cell arms protrude through the walls of the bath. The total pressure in the cell (5 – 80 Torr) was controlled via a needle valve on the exhaust line to the pump, and measured using a capacitance manometer. The bath was filled with acetone/dry ice, chloroform/dry ice, or *ortho*-xylene/dry ice to achieve sub-ambient temperatures of 195, 212 and 250 K, respectively. Temperatures close to the reaction zone were measured using K-type thermocouples.

Glyoxal was prepared by heating approximately equal masses (~ 15 g) of glyoxal trimer dihydrate crystals with P_2O_5 to 423 K. A small flow of N_2 was passed over the heated sample and through a collection trap submerged in liquid N_2. The glyoxal was collected as yellow crystals, distilled into a gas sample bulb and diluted in N_2; and typically used directly following preparation. The concentration of $(HCO)_2$ in each sample bulb was determined via UV-VIS spectroscopy.

Materials used: nitrogen (BOC oxygen free), oxygen (Air Products, high purity, 99.999%), *t*-butyl-hydroperoxide (Sigma Aldrich, 70% v/v aqueous), oxalyl chloride (Sigma Aldrich, ≥ 99%), chloroform (Sigma Aldrich, ≥ 99.8%), o-xylene (Sigma Aldrich, ≥ 98%), Acetone (Sigma Aldrich, > 99.9%), glyoxal trimer dihydrate (Sigma Aldrich, ≥ 95%), phosphorus pentoxide (Sigma Aldrich, ≥ 98.5%).

OH radicals and Cl atoms were generated by pulsed excimer laser photolysis (Lambda Physik Compex, at 248 nm) of *t*-butyl-hydroperoxide and oxalyl chloride, respectively:

$$t\text{-}C_4H_9OOH + h\nu \rightarrow OH + \text{co-products} \quad \text{(P1)}$$

$$(COCl)_2 + h\nu \rightarrow 2Cl + 2CO \quad \text{(P2)}$$

Photolysis energies were typically 30 – 100 mJ pulse^{-1}; the laser beam had an area of ~ 2 cm^2 and was introduced through one of the arms of the reactor. The laser was typically operated at 10 Hz, although tests were undertaken at lower pulse repetition rates to ensure that fresh gas samples were present in the reactor for each photolysis pulse.

OH radicals were detected by off-resonance LIF following excitation at ~ 282 nm ($A^2\Sigma(v'=1) \leftarrow X^2\Pi(v''=0)$, $Q_1(1)$) with the off-resonant fluorescence being observed at ~ 308 nm through an interference filter (Barr Associates, 308 ± 5 nm) by a photomultiplier tube mounted perpendicular to the plane of the photolysis and probe laser beams. Probe radiation was generated from a YAG pumped (Continuum Powerlite 8010) dye laser (Spectra Physics PDL-3) operating on Rhodamine6G dye. The photomultiplier signal was integrated using a boxcar averager (SRS) and digitized before being passed to a computer for data analysis. The time delay between photolysis and probe laser pulses was controlled by a digital delay generator and varied in order to build up a time dependent OH profile following photolysis. Kinetic traces were typically 200 data points each averaged 5 – 10 times dependent on the signal-to-noise ratio.

The reactions were carried out under pseudo-first-order conditions with glyoxal concentrations (> 9×10^{13} molecule cm^{-3}) in great excess over OH (~ 1×10^{11} molecule cm^{-3}). In N_2 bath gas the OH decay is governed by reactions 2 and 7:

$$(HCO)_2 + OH \rightarrow HC(O)CO + H_2O \quad \text{(R2)}$$

$$OH \rightarrow \text{Loss} \quad \text{(R7)}$$

where reaction 7 accounts for reaction with *t*-butyl-hydroperoxide and diffusion from the probed region of the reactor. Under these conditions the OH decay, an example of which is shown in the inset of Figure 2, is defined using the following expression:

$$I_f(t) = I_f(0) \exp^{-k't} \quad \text{(E1)}$$

where $I_f(0)$ and $I_f(t)$ are OH signals at time 0 and time *t*, respectively; and $k' = k_2[(HCO)_2] + k_7$. Accordingly, the gradient of a linear plot of k' against $[(HCO)_2]$ provides the bimolecular rate coefficient, k_2; an example of which can be seen in the upper line of Figure 2.

In excess O_2 the rate of OH decay slows relative to that measured in N_2 (see lower line in Figure 2), which we assigned to rapid recycling through reaction 6. Provided the rates of reactions 3 and 6 are fast compared to the OH + $(HCO)_2$ reaction, then HC(O)CO can be considered in a steady state; OH loss is determined by the fraction of total HC(O)CO loss that does not recycle OH, and defined by the following rate law:

$$-\frac{d[OH]}{dt} = k'_2[OH] - k'_6[HC(O)CO] + k_7[OH] \quad \text{(E2)}$$

where $k'_2 = k_2[(HCO)_2]$ and $k'_6 = k_6[O_2]$. As HC(O)CO is in the steady state:

$$k'_2[OH] = (k'_6 + k_3)[HC(O)CO] \quad \text{and}$$

$$-\frac{d[OH]}{dt} = k'_2[OH]\left(1 - \frac{k'_6}{k'_6 + k_3}\right) + k_7[OH] \qquad \text{(E3)}$$

The bimolecular rate coefficient measured in the presence of O_2, k_{O2}, is lower than the bimolecular rate coefficient measured in pure N_2, where ($k_{N2}=k_2$), by a factor $\left(1 - \frac{k'_6}{k'_6 + k_3}\right) = \frac{k_{O2}}{k_{N2}}$.

The OH yield, $\Phi_{OH,}$ is given by:

$$\Phi_{OH} = \frac{k_6[O_2]}{k_6[O_2] + k_3} \qquad \text{(E4)}$$

Therefore the experimental Φ_{OH} can be determined by the ratio of rate coefficients measured in the presence and absence of O_2:

$$\Phi_{OH} = 1 - \frac{k_{O2}}{k_{N2}} \qquad \text{(E5)}$$

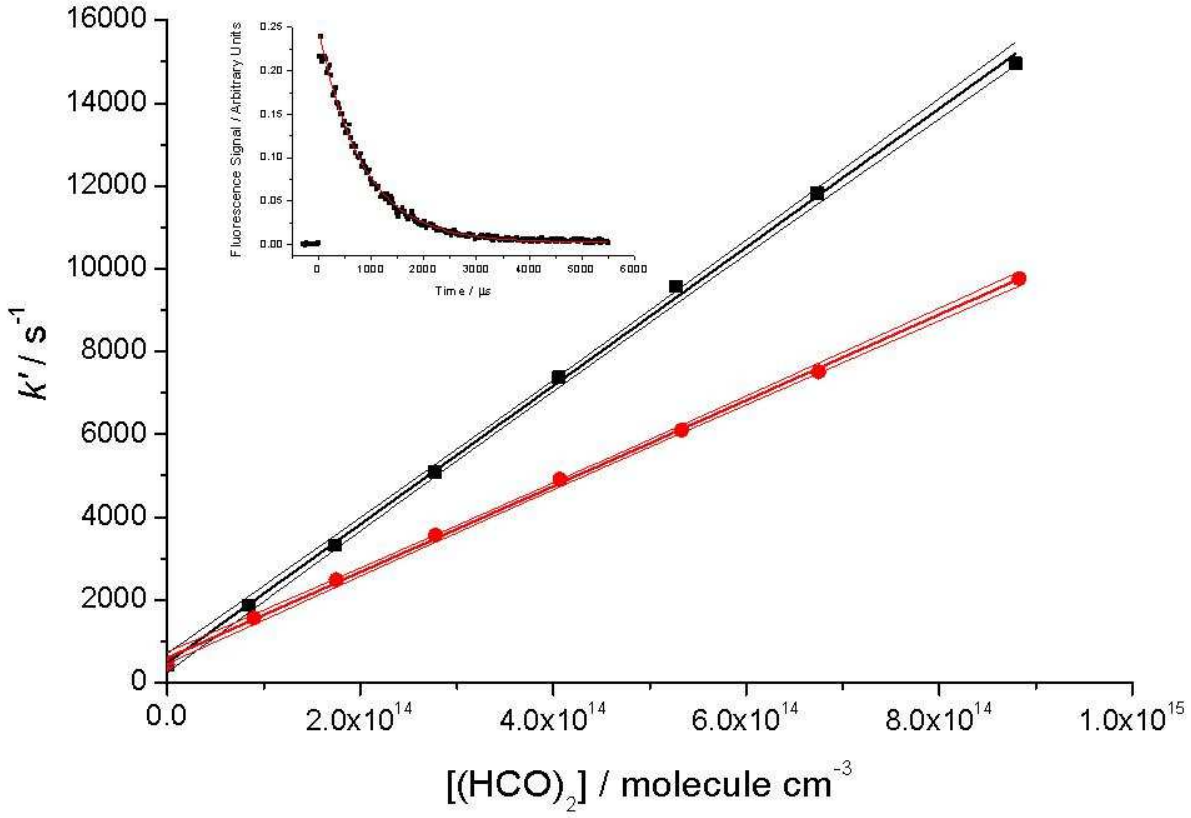

Figure 2. Bimolecular plots for the OH + $(HCO)_2 \rightarrow$ Products reaction at 212 K and 40 Torr total pressure; in pure N_2 (■), and in the presence of 869 mTorr of O_2 (●). The outer lines show the confidence intervals at the 2σ level. A typical experimental OH decay and fit to equation E1 is shown in the insert.

Results and Discussion

OH + $(HCO)_2$ Temperature dependence in N_2 bath gas

Rate coefficients, $k_2(T)$, were determined under pseudo-first-order condition in OH over the temperature range 212-295 K, and total pressures ranging from between 5 and 80 Torr in N_2 bath gas. $k_2(T)$ was found to be independent of total pressure, consistent with a reaction proceeding via H-atom abstraction at either aldehydic group. The experimental $k_2(T)$ measurements are highly reproducible, with values of (9.7 ± 1.2), (12.2 ± 1.6) and (15.4 ± 2.0) × 10^{-12} cm^3 $molecule^{-1}$ s^{-1} at temperatures of 295, 250 and 212 K respectively,

obtained by averaging all independent measurements (>11) at each temperature. The error is the statistical error combined in quadrature with an estimated 10% systematic error. To our knowledge, the only previous experimental investigation of the temperature dependence of $k_2(T)$ reported in the literature is that by Feierabend et al.[17] These authors measured $k_2(T)$ over a range of total pressures (45-300 Torr) and temperatures (210-390 K) in both N_2 and He bath gas, and found experimental rate coefficients independent of bath gas or total pressure. The work by Feierabend et al. yields a room temperature k_2(296 K) of (9.15 ± 0.80) × 10^{-12} cm^3 $molecule^{-1}$ s^{-1}; furthermore, $k_2(T)$ was found to demonstrate a negative temperature dependence with slightly non-Arrhenius behaviour over their experimental temperature range. Plum et al.[38] measured k_2(296 K) by a relative rate method in air, using the OH + cyclohexane reaction as reference, and reported a value of (11.5 ± 0.4) × 10^{-12} cm^3 $molecule^{-1}$ s^{-1}, assuming the reference reaction occurs at a rate of 7.57 × 10^{-12} cm^3 $molecule^{-1}$ s^{-1}. Feierabend et al. pointed out that using the recently recommended room temperature rate for the OH + cyclohexane reaction of 7.17 × 10^{-12} cm^3 $molecule^{-1}$ s^{-1}, reduces the Plum et al. k_2(296 K) value to (10.90 ± 0.40) × 10^{-12} cm^3 $molecule^{-1}$ s^{-1}. Note that because Plum et al. used a relative rate technique, monitoring the consumption of glyoxal (and reference), their results would be unaffected by the OH recycling that would be occurring. Figure 3 shows the temperature dependent $k_2(T)$ values measured during this work, alongside other $k_2(T)$ values reported in the literature; a table of all experimental values measured during this work is provided in the supplementary information (Table S1).

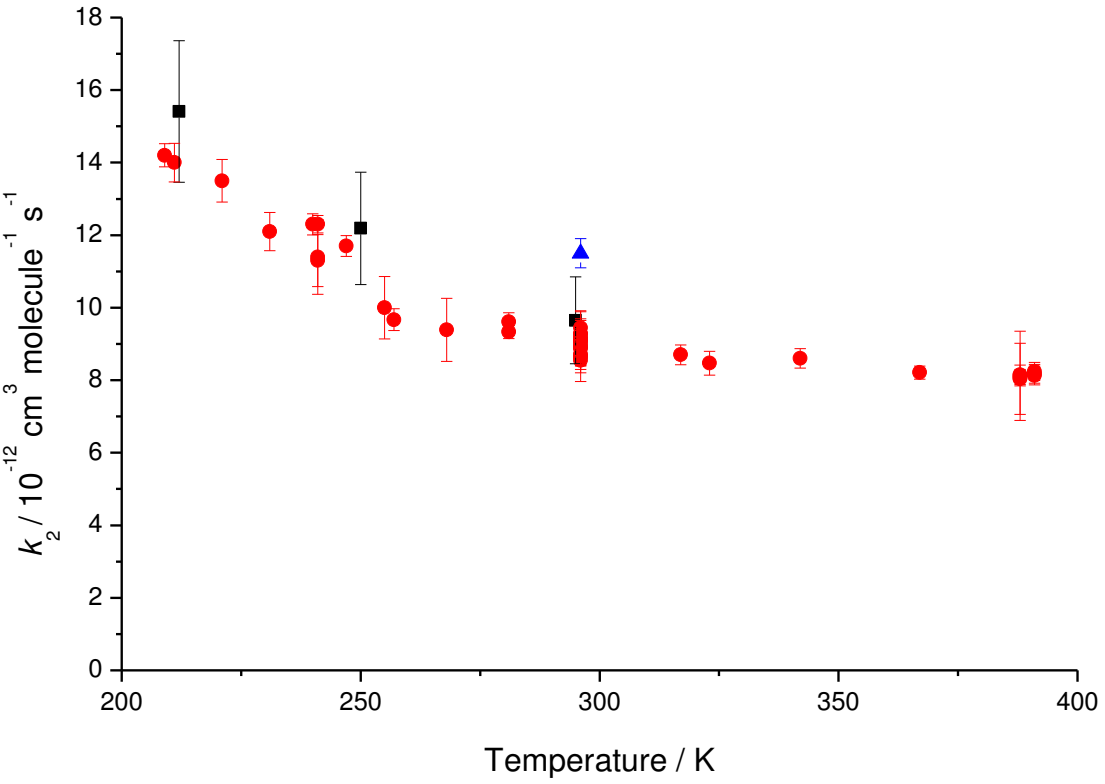

Figure 3. Temperature dependence of the OH + $(HCO)_2$ rate coefficient, $k_2(T)$, measured between 5 and 80 Torr total pressure using N_2 bath gas (■); the error bars include both the statistical (2σ level) and estimated systematic error. The $k_2(T)$ values measured by Feierabend et al.[17](●), and the room temperature k_2(296 K), relative rate value reported by Plum et al.[38] (▲) are included for comparison.

The experimental $k_2(T)$ values measured here lie in reasonable agreement with values reported in the literature, and give confidence in our understanding of the OH + $(HCO)_2$ system using an inert bath gas. The observed scatter in k_2 values at fixed temperatures are attributed to systematic errors associated with the experiment. It is worthwhile to note that the scatter observed in k_2 measurements does not influence the experimental OH yield measurements, as these are based on the relative change in k_2 following addition of O_2 to the reactor (Equation 5), and not on absolute k_2 values. Furthermore, OH decay traces using pure N_2 bath gas were recorded at the beginning and end of each day of experiments to ensure that the $k_2(T)$ measurement had remained constant.

Generation of OH from the HC(O)CO + O_2 reaction

Preliminary experiments to demonstrate primary OH production were conducted generating the HC(O)CO radical via Cl-atom initiated oxidation of $(HCO)_2$

$$(HCO)_2 + Cl \rightarrow HC(O)CO + HCl \quad \text{(R8)}$$

in the presence of O_2 over a range of total pressures (5-20 Torr) and temperatures (195 and 295 K); OH production could then be monitored directly by LIF. OH growth was observed under all experimental conditions, a typical OH profile is presented in Figure 4. Tests were carried out that confirmed OH growth was not observed in the absence of Cl-atom precursor or O_2. While these experiments do not allow the rate or yield of OH to be quantified, they do provide insight as to which of the proposed reaction schemes are responsible for OH formation. Niki et al.[19] proposed that reaction of $HC(O)C(O)O_2$ radicals with HO_2 could potentially result in OH production (Reaction 5); in a reaction scheme that also involved self reaction of $HC(O)C(O)O_2$ peroxy radicals (R9) and unimolecular decomposition of the resulting HC(O)C(O)O alkoxy radical (R10):

$$2HC(O)C(O)O_2 \rightarrow 2HC(O)C(O)O + O_2 \quad \text{(R9)}$$

$$HC(O)C(O)O \rightarrow HCO + CO_2 \quad \text{(R10)}$$

The initial Cl-atom concentration, $[Cl]_0$, generated in the reactor was estimated using:

$$[Cl]_0 = \sigma_{248\ nm}\Phi_{Cl,248\ nm}F[(COCl)_2]_{LIF} \quad \text{(E6)}$$

to be of the order ~ 1×10^{13} atom cm^{-3} under our experimental conditions, where σ_{248nm} and $\Phi_{Cl,248nm}$ are the absorption cross section and Cl-atom quantum yield for oxalyl chloride photolysis at 248 nm,[39] *F* is the photolysis laser fluence, and $[(COCl)_2]_{LIF}$ is the concentration

of precursor in the reactor. Conversely, da Silva[21] proposed OH radicals form directly following reaction of HC(O)CO radicals with O_2 in a chemically activated pathway (Reaction 6); in excess O_2 this channel is consistent with the observed OH formation on the microsecond timescale. The numerical programme KINTECUS[40] was used to simulate experimental OH profiles for the Cl + $(HCO)_2/O_2$ reaction at 295 K and 10 Torr total pressure, as defined by either the Niki et al.[19] or da Silva[21] mechanism as shown in Figure 4.

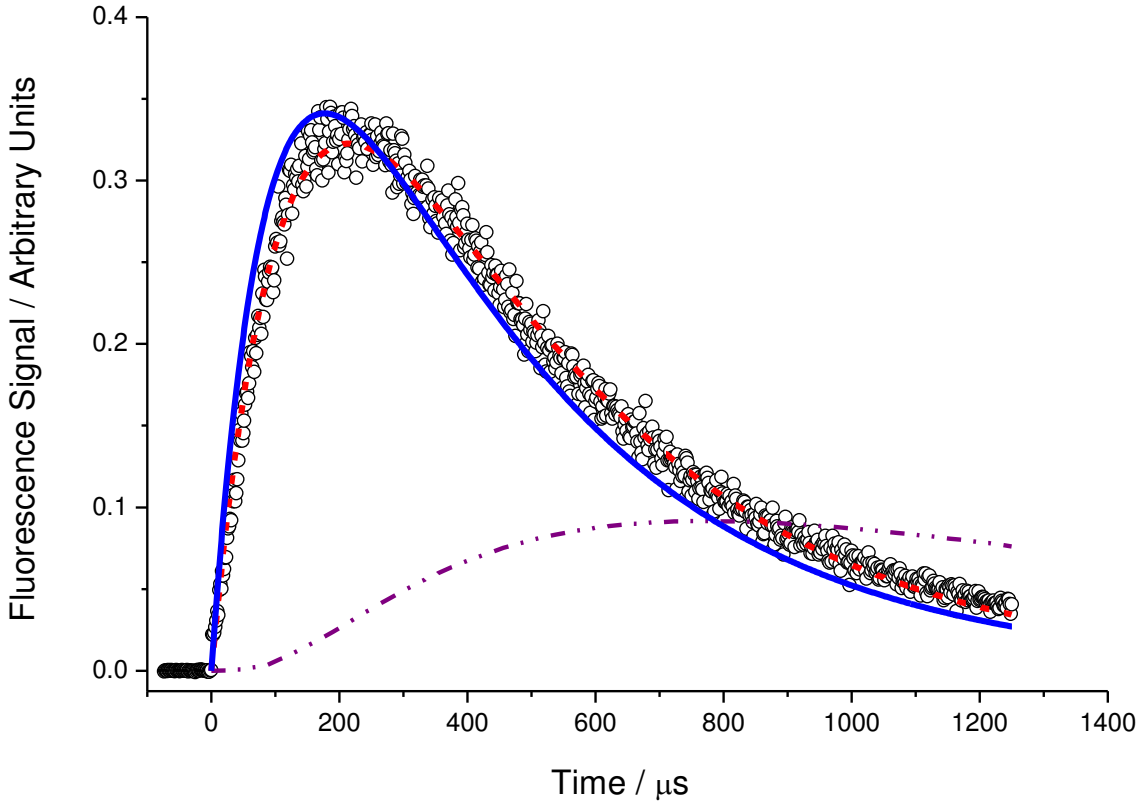

Figure 4. Experimental OH profile (open circles) following the Cl + $(HCO)_2$ reaction in the presence of 1.04×10^{17} molecule cm^{-3} O_2 at 295 K and 10 Torr total pressure. Three model simulations are included. 1) Blue solid line using the OH pathways proposed by da Silva[21] and the Cl + glyoxal rate coefficient reported by Niki et al. The fit is qualitatively very good. 2) Red dashed line, best fit to the experimental data floating rate coefficents in the da Silva mechanism and Cl + glyoxal (see text for details). 3) The lower purple dashed-dot line shows a simulation based on the Niki et al.[19] mechanism for OH formation where there is a clear induction period before OH generation and peak OH occurs much later than the experimental observations.

Radical-radical reactions are too slow to contribute to the observed chemistry given the magnitude of the estimated initial Cl-atom concentration in the reactor, and hence the Niki et al. reaction scheme fails to reproduce the experimental time dependent OH profile, even when rate coefficients for Reactions 5 and 9 are allowed to achieve the gas-kinetic collision rate. The red dashed line in Figure 4 shows the optimised fit through the experimental data using the da Silva mechanism, with k_6 fixed at 5×10^{-12} cm^3 molecule^{-1} s^{-1} and rate coefficients for reactions 2, 3 and 8 all allowed to float; the blue line shows the fit using the same mechanism but with k_8 fixed at 3.8×10^{-11} cm^3 molecule^{-1} s^{-1}, the experimental value reported by Niki et al. Tables showing the rate coefficient values used in each fitting routine are provided in the supplementary information (Tables S2, S3). Direct observation of OH following the Cl + $(HCO)_2/O_2$ reaction provides strong evidence that reaction of the HC(O)C(O) radical with O_2 proceeds directly to OH + CO_2 + CO, as proposed by recent theoretical calculations by da Silva.[21]

Experimental OH Yields for the OH + $(HCO)_2/O_2$ reaction

OH yields for the OH + $(HCO)_2/O_2$ system have been quantified over a range of experimental temperatures (212 – 295 K) and total pressures (5 – 80 Torr), from the ratio of rate coefficients measured in the presence and absence of O_2 (Equation 5). Figure 5 shows the experimental OH yield data plotted as a function of O_2 fraction, f-O_2, at 295 K and a full table of the results are presented in the supplementary information (Table S4).

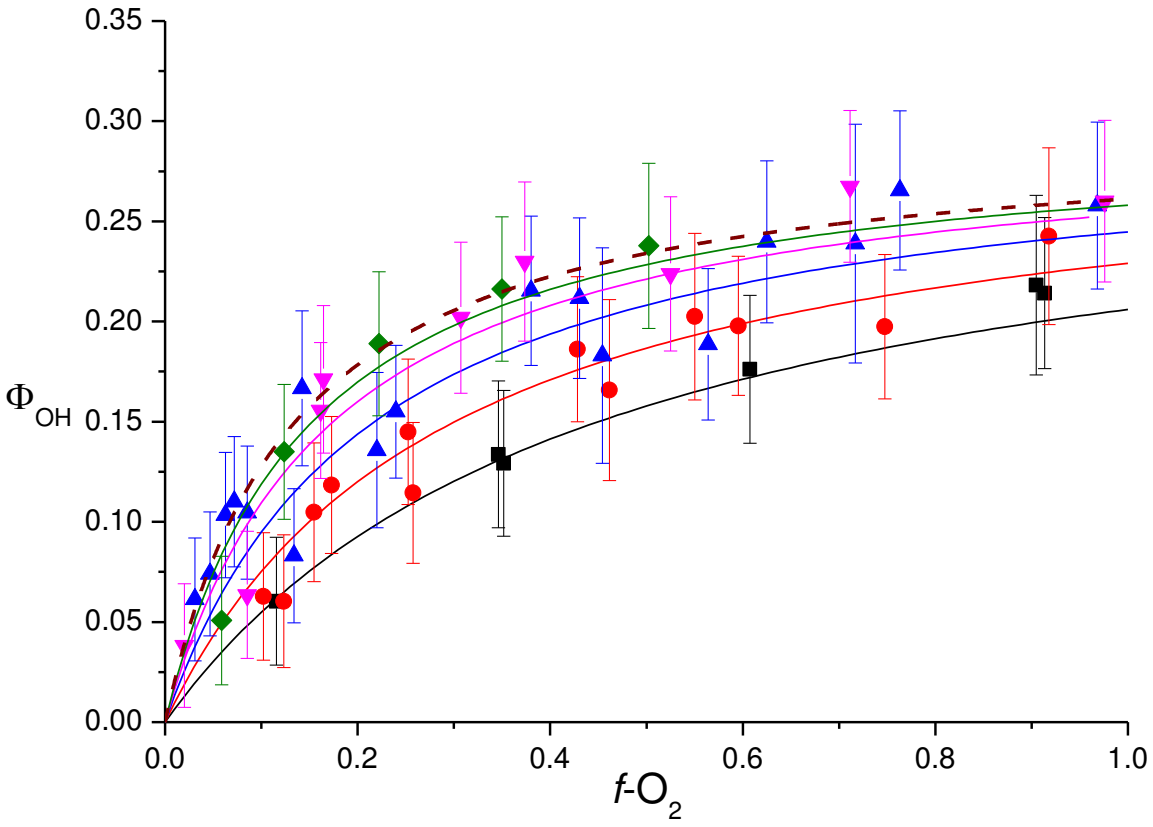

Figure 5. Experimental OH yields, ϕ_{OH}, for the OH + $(HCO)_2/O_2$ reaction at 295 K as a function of oxygen fraction, *f*-O_2, at total pressure of 5 (■), 10 (●), 20 (▲), 40 (▼) and 80 Torr (♦). The dashed line shows the predicted ϕ_{OH} dependence on *f*-O_2 at 760 Torr. The error bars include both the statistical (2σ) and estimated systematic errors. Included are fits through each total pressure data set using the extended Lindemann-Hinshelwood model (see text for details).

It can be seen that the OH yields increase with *f*-O_2 at a given pressure as reaction 6 competes with thermal decomposition (reaction 3). However, the OH yield tends to a limiting value. We interpret this observation as evidence that a fraction of the HC(O)CO radical population is formed following reaction 2 with sufficient energy to promptly dissociate, in contrast to the mechanism proposed by da Silva[21] which treats the HC(O)CO radical at thermal equilibrium. The fate of the remaining HC(O)CO population is determined

by a competition between thermal decomposition (R3) and bimolecular association with O_2 to give OH (R6).

In order to determine the limiting OH yields and to determine the OH yields as a function of pressure at atmospheric oxygen fractions (f-O_2 = 0.21), the data have been parameterised with a model based on a simple Lindemann-Hinshelwood (LH) mechanism that allows for prompt dissociation of a fraction of the chemically activated HC(O)CO radical. Unimolecular dissociation and bimolecular association reactions potentially have rate coefficients which show a dependence on pressure; the Lindemann-Hinshelwood expression for a pressure dependent rate coefficient is given by:

$$k_{LH} = \frac{[M]}{\frac{1}{k_0} + \frac{[M]}{k_\infty}} \qquad \text{(E7)}$$

where k_{LH} is the reaction rate coefficient at total pressure [M], and k_0 and k_∞ are the limiting low and high pressure rate coefficients, respectively.[41] The Lindemann-Hinshelwood model captures the physical steps involved in reaction but inadequately accounts for the internal energy of the molecule.[41,42] Here we assign Lindemann-Hinshelwood forms for the pressure dependence of both HC(O)CO decomposition and association with O_2 rate constants. This model is flexible enough to adequately paramaterise the data, but it is concluded that the system is more complex, and that limited physical significance can be assigned to the fitting parameters (see below). Complications arise because the HC(O)CO radical is formed with excess energy (exothermicity of reaction 2 ~ -130 kJ mol^{-1}), and undergoes subsequent chemistry before this excess energy is removed. This is a “chemical activation” problem, a detailed consideration of which is beyond the scope of this study, but will be addressed in a

future paper. For the present we develop a model to parameterise the system based on thermal rate constants and prompt dissociation which allows us to predict yields under atmospheric conditions. We then briefly discuss evidence for chemical activation.

The fraction of prompt HC(O)CO dissociation is accounted for in our analysis by the OH_{LIMIT} parameter, which signifies the fraction of the total HC(O)CO population that survives the OH + $(HCO)_2$ reaction. How close the OH yield system is to the OH_{LIMIT} depends on k_3 and $k_6[O_2]$, and is given by:

$$\Phi_{OH} = OH_{LIMIT}\left(\frac{k_6[O_2]}{k_6[O_2]+k_3}\right) \qquad \text{(E8a)}$$

If Lindemann-Hinshelwood forms are assigned to k_3 and k_6, then equation 8a gives:

$$\Phi_{OH} = OH_{LIMIT}\left(\frac{\left(\frac{[M][O_2]}{A^{-1}+B^{-1}[M]}\right)}{\left(\frac{[M][O_2]}{A^{-1}+B^{-1}[M]}\right)+\left(\frac{[M]}{C^{-1}+D^{-1}[M]}\right)}\right) \qquad \text{(E8b)}$$

where the *A* and *B* parameters are related to the pressure dependence in the HC(O)CO + O_2 association reaction, while the *C* and *D* parameters are related to the pressure dependent decomposition channel.

The pressure and oxygen dependent experimental OH yields have been fitted at each experimental temperature independently, using equation 8b. These OH yields only identify the ratio k_3/k_6; hence there is no unique solution for each temperature data set. In order to constrain the fit, the parameters *B* and *D*, which are related to the high-pressure limiting rates of HC(O)CO association with O_2 and decomposition, respectively, have been fixed. The *B* parameter was fixed at a value of 5×10^{-12} cm^3 $molecule^{-1}$ s^{-1}, typical of many

radical + O_2 reactions at limiting high pressure.[37,43-45] It was also assumed the *B* parameter was independent of temperature. High pressure limiting rate coefficients for HC(O)CO decomposition were calculated using an RRKM/master equation analysis with the open source MESMER computer program.[46] The zero point energy corrected barrier height for decomposition was obtained by performing geometry optimisations of HC(O)CO and the decomposition transition state and subsequent harmonic frequency analysis at the bb1k / aug-cc-pVDZ level of theory followed by single point energy calculations at the CCSD(T)/aug-cc-pVTZ level of theory using the Gaussian 09 suite of programs.[47] Collisions between the nitrogen bath gas and HC(O)CO were parameterised using a Lennard-Jones model and energy transfer was treated using an exponential down model parameterised with a temperature independent ΔE_d. Molecular densities of states were obtained assuming a rigid rotor-harmonic oscillator model and one vibration within the transition state was treated as a hindered rotation. All parameters used in these calculations are given in the supplementary information.

Room temperature Φ_{OH} measurements are presented in Figure 5 as a function of total pressure and oxygen fraction, *f*-O_2; together with analysis using this extended Lindemann-Hinshelwood model (E8b). Figure 5 shows that equation 8b adequately parameterises the data; Figures 6 and 7 show this also to be the case at the lower temperatures. Both experimental and theoretical studies have indicated that at ambient temperatures and pressures, k_3 is in its pressure dependent regime, close to the low pressure limit.[20,21,48] Therefore as the total pressure is increased, more O_2 is required for the bimolecular reaction channel (R6) to effectively compete with dissociation (Figure 5). The

analysis of all the ambient temperature Φ_{OH} measurements suggests an OH_{LIMIT} of (0.29 ± 0.03) at 295 K.

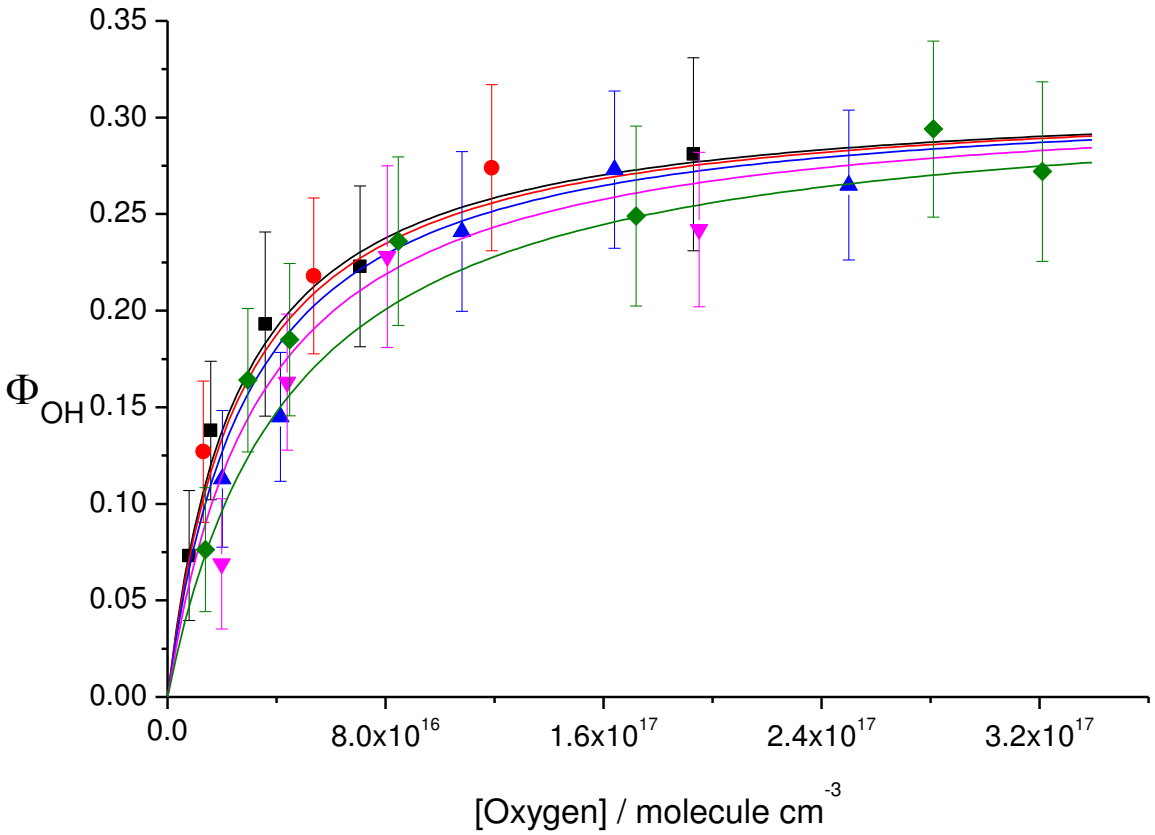

Figure 6. Experimental OH yields, Φ_{OH}, for the OH + $(HCO)_2/O_2$ reaction at 250 K as a function of oxygen concentration at total pressure of 5 (■), 10 (●), 20 (▲),40 (▼) and 80 Torr (♦). The error bars include both the statistical (2σ) and estimated systematic errors.

In contrast to the data at 295 K, the experimental OH yields measured at 250 K are independent of total pressure, but strongly dependent on the O_2 concentration; reaching an OH_{limt} of 0.31 ± 0.04. Data at 250 K are plotted in Figure 6, note here we are plotting the OH yield as a function of absolute oxygen concentration rather than *f*-O_2, the comparative plot for the 295 K data is presented in Fig S1 of the supplementary information which shows the pressure variation as a function of $[O_2]$ at 295 K. Further discussion of the data at 295 K and the role of chemical activation is presented below.

Qualitatively similar behaviour to Figure 6 is observed at 212 K (Figure 7), although less O_2 is required in order to titrate all available HC(O)CO to OH, consistent with an Arrhenius temperature dependence in k_3. The OH_{LIMIT} at 212 K increases further to 0.38 ± 0.02, suggesting an increasing fraction of the nascent HC(O)CO population form with energy in excess of the threshold to dissociation as the temperature increases. The parameters used to fit each temperature data set are presented in Table 1.

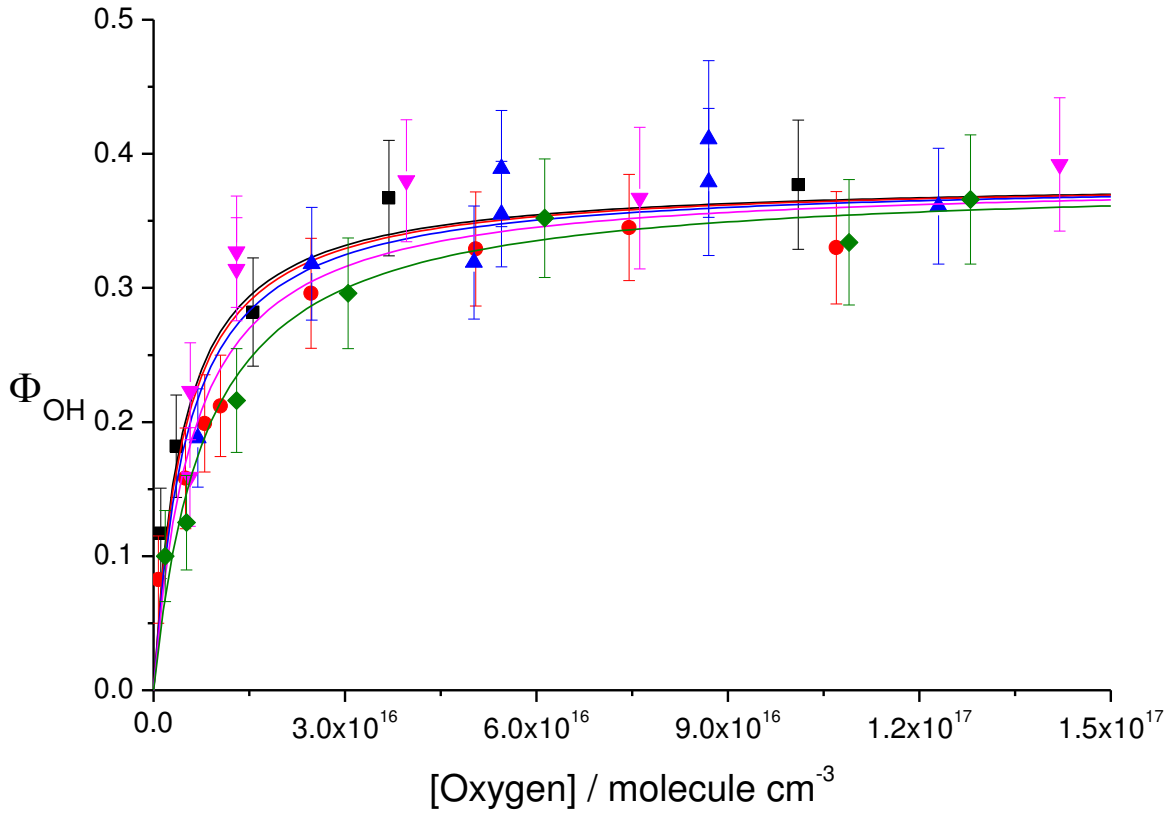

Figure 7. Experimental OH yields, Φ_{OH}, for the OH + $(HCO)_2/O_2$ reaction at 212 K as a function of oxygen concentration at total pressure of 5 (■), 10 (●), 20 (▲),40 (▼) and 80 Torr (◆). The error bars include both the statistical (2σ) and estimated systematic errors.

Parameter	Temperature / K		
	295	250	212
OH_{LIMIT}	0.29 ± 0.03	0.31 ± 0.04	0.38 ± 0.03
A	$(12.0 \pm 4.8) \times 10^{-30}$ cm^3 molecule^{-1} s^{-1}	$(14.0 \pm 9.6) \times 10^{-31}$ cm^3 molecule^{-1} s^{-1}	$(12.9 \pm 7.5) \times 10^{-31}$ cm^3 molecule^{-1} s^{-1}
B	5×10^{-12} cm^3 molecule^{-1} s^{-1}	5×10^{-12} cm^3 molecule^{-1} s^{-1}	5×10^{-12} cm^3 molecule^{-1} s^{-1}
C	$(5.6 \pm 1.2) \times 10^{-13}$ s^{-1}	$(3.4 \pm 1.2) \times 10^{-14}$ s^{-1}	$(5.4 \pm 1.6) \times 10^{-15}$ s^{-1}
D	2.6×10^{9} s^{-1}	3.0×10^{8} s^{-1}	2.4×10^{7} s^{-1}

Table 1. Parameters used to model experimental OH yields, Φ_{OH}, for the OH + $(HCO)_2/O_2$ reaction as a function of total pressure and temperature. See text for information on the values for fixed parameters *B* and *D*.

Ambient OH yields

The parameters used to describe the OH yields observed for the OH + $(HCO)_2/O_2$ system under the experimental conditions considered here, have been used to predict the OH yield dependence on temperature and total pressure using an *f*-O_2 of 0.21, and suggest that at total pressures relevant to the troposphere the OH yields predicted at 295, 250 and 212 K are 0.19, 0.30 and 0.38, respectively (Figure 8); the OH yield predicted at 295 K using pure O_2 is included in Figure 8 (dashed black line), and confirms a significant contribution from both chemically activated and thermal HC(O)CO dissociation under tropospheric conditions. At 760 Torr and 295 K, our calculated OH yield, based on experimental measurements, of ~ 0.19 is approximately a factor two greater than predicted from the calculations of Setokuchi.[22] da Silva[21] calculates a significantly higher OH yield of 0.36 under tropospheric conditions, with very little stabilisation to $HC(O)C(O)O_2$, and with decomposition accounting for the vast majority of the balance of 0.64. However, as noted before, da Silva considered only a thermal distribution of HC(O)CO radicals.

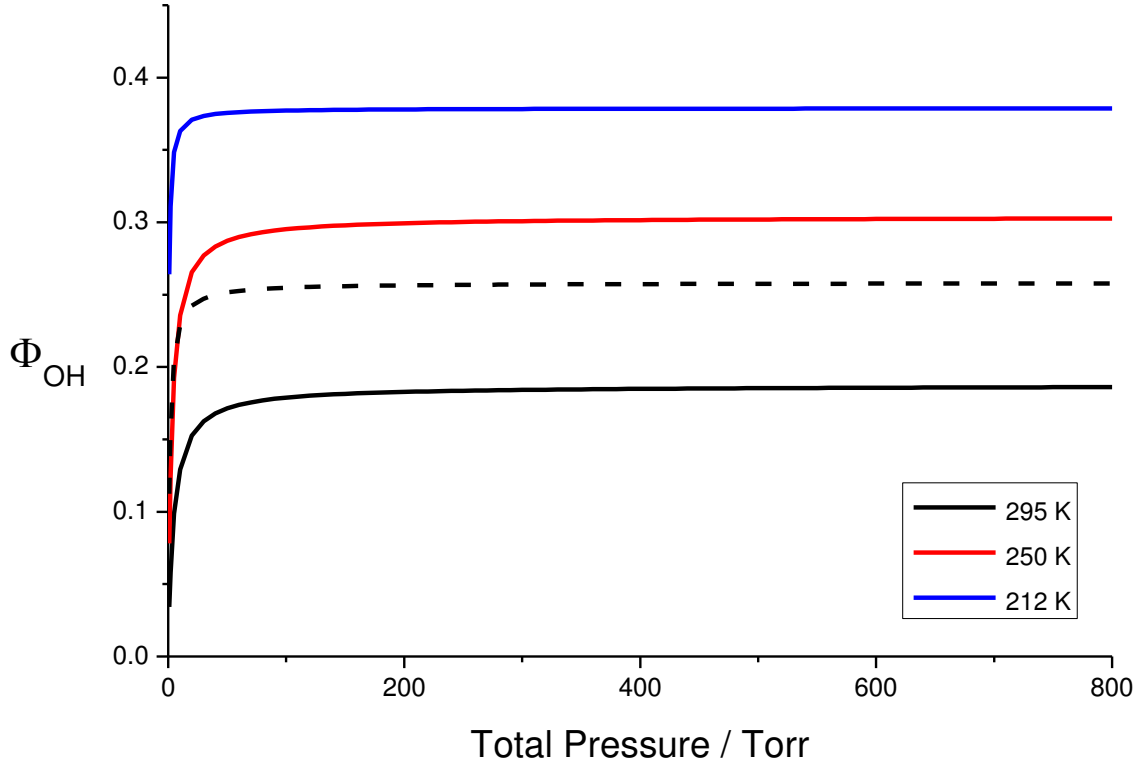

Figure 8. OH yields as a function of temperature and total pressure at atmospheric oxygen mixing ratios (f-O_2 = 0.21); included are the OH yields predicted at 295 K in pure O_2 (dashed line).

Evidence for non-thermal rate behaviour

As the OH yields are essentially pressure independent at 250 and 212 K (Figures 6 and 7), both k_3 and k_6 might be assumed to be approaching their high-pressure limits at these temperatures; indeed, master equation calculations on k_6 performed as part of this work and by da Silva[21], suggest that k_6 should be pressure independent at just a few Torr total pressure. However, satisfactory fits through the 250 and 212 K data sets constraining k_3 to the high-pressure limit values of 3×10^{8} and 2.4×10^{7} s^{-1} (Table 1), respectively, require k_6 values of 1×10^{-8} cm^3 and 5×10^{-9} $molecule^{-1}$ s^{-1} at 250 and 212 K, respectively, which exceed the gas-kinetic collision rate by several orders of magnitude. Alternatively, given that

k_6 is calculated to be pressure independent at all experimental temperatures and pressures, attempts were made to fit the complete data set by allowing only k_3 to be pressure dependent, but poor quality fits were obtained. Our experimental results indicate that pressure dependence in both k_3 and k_6 is required to fit the data.

However, if both k_3 and k_6 are allowed to vary according to the Lindemann-Hinshelwood mechanism, then the *A* parameter (Table 1) shows anomalous behaviour if it is interpreted as the low-pressure limiting rate constant for k_6. Low-pressure rate constants for association reactions increase as the temperature decreases because of the increased lifetime of the activated adduct whereas our data predicts the opposite behaviour for *A*. The observations suggest that the system is not described by thermal rate constants.

Further evidence for non-thermal behaviour comes from a consideration of the ratio of k_3/k_6. It follows from equation 8a that the OH_{LIMIT}/Φ_{OH} ratio should scale linearly with the inverse O_2 concentration, with a gradient equal to the k_3/k_6 ratio and an intercept of 1 (see also the comparison with Orlando and Tyndall[20] data below). Figure 9 shows such a plot at 295 K at selected pressures. The k_3/k_6 ratios derived following linear analysis of the OH yields observed at all experimental pressures at 295 K are presented in Figure 10 as a function of total pressure; a table of these values is included in the supplementary information (Table S5). The solid line in Figure 10 is the ratio of thermal rate coefficients calculated in MESMER. Given that k_6 is essentially at the high pressure limit, this maps out the pressure dependence of k_3. As the total pressure is increased above 20 Torr, the observed k_3/k_6 ratio increases with total pressure, indicating that k_3 increases more rapidly with total pressure than k_6 as predicted by the calculations. However, below 20 Torr, the

k_3/k_6 ratio appears pressure independent, suggesting that k_3 is faster than expected under these conditions due to the effect of chemical activation.

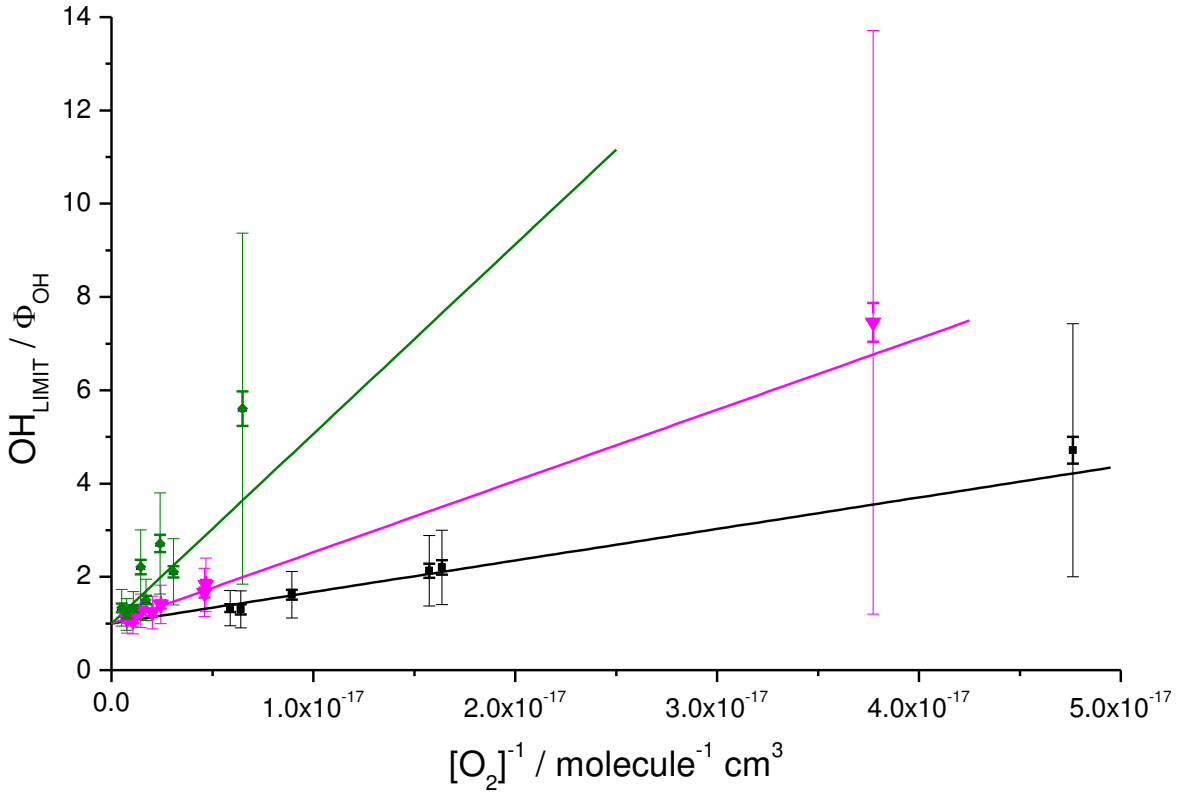

Figure 9. Ratios of the observed OH_{LIMIT}/Φ_{OH} following glyoxal oxidation as a function of inverse O_2 concentration at 5 (■), 40 (▼) and 80 (♦) Torr total pressure and 295 K; the small error bars are purely statistical (2σ); the larger error bars include the estimated systematic error.

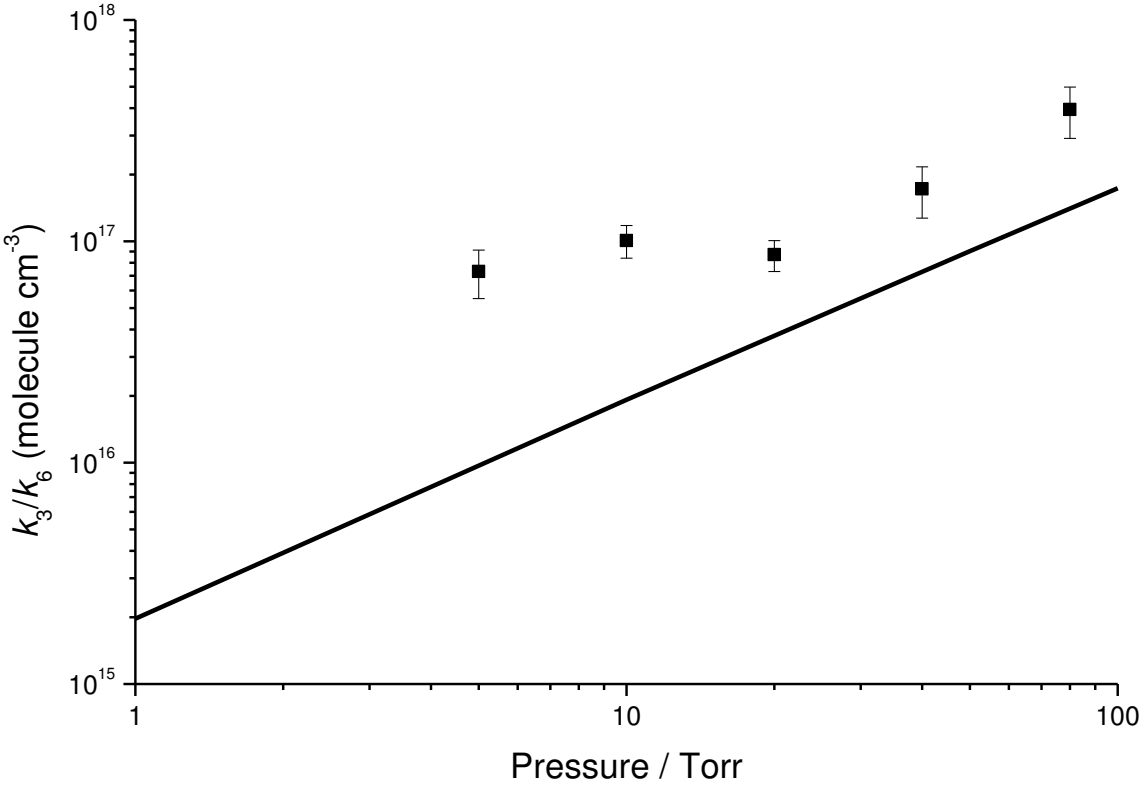

Figure 10. The observed k_3/k_6 ratio dependence on total pressure (5 – 80 Torr) at 295 K. The solid line is the k_3/k_6 ratio calculated by MESMER based on thermal rate coefficients for k_3 and k_6 suggesting a linear dependence to pressures of ~ 1 Torr.

Linear dependence of $[CO]/[CO_2]$ *products as a function of* $1/[O_2]$

Orlando and Tyndall[20] carried out an extensive investigation of HC(O)CO chemistry over a range of temperatures (224 – 317 K) at near atmospheric pressure, during chamber experiments coupled with FTIR product detection. Analysis by these authors was based on the mechanism proposed by Niki et al.[19], and reported a strong linear dependence of the $[CO]/[CO_2]$ ratio on the inverse O_2 partial pressure (Figure 11). Our data show a similar behaviour (Figure 6), as OH_{LIMIT}/Φ_{OH} is directly related to $[CO]/[CO_2]$; to assert the credibility of the mechanism proposed here, similar behaviour must be predicted.

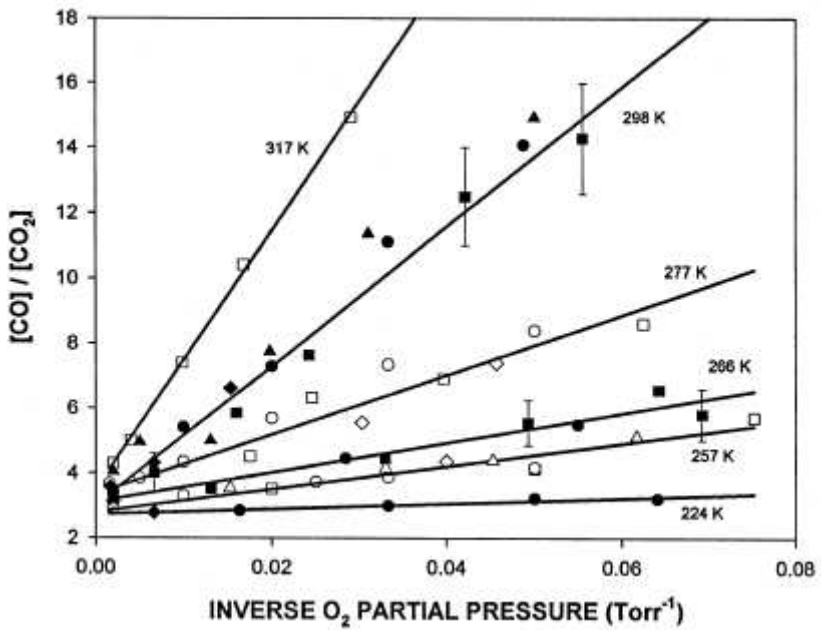

Figure 11. Observed $[CO]/[CO_2]$ ratios from glyoxal oxidation as a function of inverse O_2 partial pressure and temperature at 700 Torr total pressure. Squares: Data obtained from photolysis of Cl_2/glyoxal/O_2/N_2 mixtures. Circles: Data obtained from photolysis of Cl_2/glyoxal/NO/O_2/N_2 mixtures. Triangles: Data obtained from photolysis of C_2H_5ONO/glyoxal/NO/O_2/N_2 mixtures. Diamonds: Data obtained from photolysis of Cl_2/glyoxal/NO_2/O_2/N_2 mixtures. (From Orlando and Tyndall[20])

In our mechanism, the HCO radicals that form following both prompt and thermal dissociation of the HC(O)CO radical, will be rapidly converted to HO_2 and CO in excess O_2 via reaction 11:

$$HCO + O_2 \rightarrow CO + HO_2 \qquad \text{(R11)}$$

Defining the term α as the fraction of the HC(O)CO population that decompose promptly before the possibility of reaction with O_2, it follows that:

$$[CO]_{prompt} = 2\alpha[HC(O)CO]_0 \qquad \text{(E9)}$$

$$[CO]_{thermal} = (1-\alpha)[HC(O)CO]_0 \left(\frac{2k_3}{k_3 + k_6[O_2]} + \frac{k_6[O_2]}{k_3 + k_6[O_2]} \right) \qquad \text{(E10)}$$

$$[CO_2]_{thermal} = (1-\alpha)[HC(O)CO]_0\left(\frac{k_6[O_2]}{k_3 + k_6[O_2]}\right) \quad \text{(E11)}$$

The subscripts 'prompt' and 'thermal' refer to the mechanism for HCOCO decomposition. Assuming the $[CO]/[CO_2]$ ratios observed by Orlando and Tyndall are defined by Equation 12:

$$\frac{[CO]}{[CO_2]} = \frac{[CO]_{prompt} + [CO]_{thermal}}{[CO_2]_{thermal}} \quad \text{(E12)}$$

then the following expression can be derived from Equations 9 – 12:

$$\frac{[CO]}{[CO_2]} = \left(\frac{2k_3}{k_6(1-\alpha)}\right)\frac{1}{[O_2]} + \left(\frac{1+\alpha}{1-\alpha}\right) \quad \text{(E13)}$$

Therefore the mechanism proposed here does predict a linear dependence of $[CO]/[CO_2]$ ratios with inverse O_2 partial pressure (with a gradient equal to $\frac{2k_3}{k_6(1-\alpha)}$ and an intercept equal to $\frac{1+\alpha}{1-\alpha}$), consistent with experimental measurements by Orlando and Tyndall. These authors reported the intercept to increase with temperature from (2.8 ± 0.4) to (3.1 ± 0.4) from 224 to 317 K, respectively; although these results were not deemed statistically significant. These observations suggest that α increases with temperature (as defined by Equation 13), or alternatively OH_{LIMIT} decreases with temperature, consistent with the results reported here. Orlando and Tyndall observed the slopes of $[CO]/[CO_2]$ vs $1/O_2$ plots to increase with temperature (Figure 11), which they attributed to a strongly Arrhenius temperature dependence of k_3. The gradient predicted using the mechanism proposed here (Equation 13) is again consistent with the observed increased gradient with temperature, given that both k_3 and α are shown to increase with temperature, and k_6 is presumed to lack

a strong temperature dependence. Orlando and Tyndall observed [CO]/[CO_2] ratios independent of inverse O_2 partial pressure at 224 K and concluded that unimolecular dissociation is unable to compete with reaction with O_2 under these conditions. Given that the minimum O_2 concentration used during these experiments is estimated to be $\sim 6.5 \times 10^{17}$ molecule cm^{-3}, more than enough to titrate all available HC(O)CO out to CO_2 via Reaction 6, these results are also in strong agreement with the results presented here.

It is worthwhile to note that during the work of Orlando and Tyndall[20], experiments were conducted in the presence of NO_2 to ascertain whether or not glyoxal derived peroxy radicals, $HC(O)C(O)O_2$ could react with NO_2 to give an acyl peroxynitrate species, analogous to the peroxyacetyl nitrate (PAN) formed through reaction of acetyl peroxy radicals with NO_2 (Reaction 12); no experimental evidence for the PAN like species, $HC(O)C(O)O_2NO_2$ could be found even at the lowest experimental temperatures.

$$CH_3C(O)O_2 + NO_2 \rightarrow CH_3C(O)O_2NO_2 \qquad (R12)$$

These observations are again consistent with HC(O)CO + O_2 chemistry occurring via an open channel out to OH, rather than collisional stabilisation into the $HC(O)C(O)O_2$ peroxy well.

Comparison of the OH/Glyoxal/O_2 and OH/Methylglyoxal/O_2 systems

It is interesting to contrast this work on glyoxal with our earlier studies on the reaction of OH with methylglyoxal.[34] Abstraction from methylglyoxal is predicted to proceed exclusively via abstraction of the aldehydic H and the resulting peroxy radical formed following the addition of O_2 ($CH_3C(O)C(O)O_2$) might be expected to undergo a similar internal abstraction

to $CH_2C(O)C(O)O_2H$ and subsequent fragmentation to give OH (+ CO_2 and HCHO). However, whilst OH recycling in the presence of O_2 was observed, the pressure dependence of the OH yield closely matched that of acetyl + O_2.

The difference in mechanism relates to the much faster rate of decomposition of $CH_3C(O)CO$ compared to HC(O)CO. The decomposition kinetics of the R-CO carbonyl radicals have been calculated by Mereau et al.[48] The thermal decomposition of $CH_3C(O)CO$ at one atmosphere is calculated to be a factor of 40 faster than that of HC(O)CO. As the pressure is lowered, HC(O)CO will enter the fall-off region before $CH_3C(O)CO$ further increasing this ratio. Jagiella and Zabel[49] measured a rate coefficient of 1.1×10^8 s^{-1} for $CH_3C(O)CO$ decomposition (measured relative to reaction with O_2 and assuming $k_{O2} = 5 \times 10^{-12}$ cm^3 $molecule^{-1}$ s^{-1}) where $CH_3C(O)CO$ was formed by the endothermic reaction of Br atoms with methylglyoxal. At the typical O_2 concentrations of our earlier work, $\sim 10^{16} – 10^{17}$ molecule cm^{-3}, thermal decomposition will be a factor of 200 – 2000 times faster than peroxy radical formation. Additionally, as discussed in the earlier work, the $CH_3C(O)CO$ is formed from the significantly exothermic OH reaction with methylglyoxal and hence prompt dissociation dominates. OH recycling is the result of the reaction of O_2 with the acetyl (CH_3CO) radicals formed from the decomposition.[50]

Atmospheric Implications

The dominant processes responsible for atmospheric removal of $(HCO)_2$ are photolysis and reaction with OH. The HC(O)CO radicals that form following reaction with OH either dissociate to HCO + CO, or react with O_2 to give CO_2, CO and OH directly. The HCO radicals

produced through photolysis and decomposition react rapidly with O_2 to give HO_2 and CO. The dissociation channel is net HO_x neutral as OH is consumed in generating the HC(O)CO radical, and HO_2 then produced through secondary chemistry. The bimolecular channel also consumes one OH in generating the HC(O)CO radical, but produces one OH through reaction with O_2. While both the unimolecular and bimolecular channels are net HOx neutral, the HC(O)CO + O_2 reaction recycles OH as OH without conversion to HO_2, and therefore acts to increase the OH/HO_2 ratio. Chemical models require reaction channels such as this to resolve the discrepancy between measured and modelled HOx concentrations in remote pristine atmospheres. Reaction with OH typically accounts for 14 – 23% of total $(HCO)_2$ removal under tropospheric conditions,[18] of which only a fraction, see Figure 8, directly regenerates OH through reaction of HC(O)CO with O_2. Therefore this chemistry only contributes a minor amount to increased OH in pristine forested environments, and the very large missing OH source reported in the literature remains unresolved.

The Master Chemical Mechanism (MCM)[51] used to describe the chemical degradation of tropospheric volatile organic compounds, currently defines HC(O)CO chemistry using the mechanism proposed by Niki et al.[19] The MCM currently treats the $HC(O)C(O)O_2$ + HO_2 reaction as comprising three competing channels. In addition to the OH forming channel proposed by Niki et al., are a peracid species, and ozone forming channels; analogous to acetylperoxy + HO_2 chemistry.[52,53] The work presented here suggests that the MCM should be amended to include direct OH formation following the HC(O)C(O) + O_2 reaction, with limited formation of $HC(O)C(O)O_2$ from OH initiated oxidation of glyoxal.

As mentioned previously, chemical activation is known to influence the product distributions observed following OH initiated oxidation of alkynes, through chemistry

initiated via OH addition.[5] Here, we have shown the influence of chemical activation may be extended to the OH + $(HCO)_2/O_2$ system, with chemistry initiated by an H-abstraction channel.

Acknowledgements

This work was supported by NERC via the grant 'Reducing the Uncertainties in Ozone Formation', through NCAS (MAB, DEH and PWS) and via a studentship to JL and via EPSRC grant EP/J010871/1.

Supporting Information available

Tables of the rate coefficients for OH + glyoxal in nitrogen (Table S1), mechanisms of the OH production from Cl initiated oxidation (Tables, S2, S3), summaries of OH yields (Table S4) and k3/k6 ratios (Table S5) are presented in the supplementary information (SI). The SI also contains an example MESMER input file for the calculations described in the text. This material is available free of charge via the Internet at http://pubs.acs.org.

References

(1) Carter, W. P. L.; Atkinson, R. Development and Evaluation of a Detailed Mechanism for the Atmospheric Reactions of Isoprene and NOx. *Int. J. Chem. Kinet.* **1996**, *28*, 497-530.

(2) Atkinson, R.; Aschmann, S. M.; Arey, J.; Carter, W. P. L. Formation of Ring-Retaining Products from the OH Radical-Initiated Reactions of Benzene and Toluene. *Int. J. Chem. Kinet.* **1989**, *21*, 801-827.

(3) Tuazon, E. C.; Macleod, H.; Atkinson, R.; Carter, W. P. L. Alpha-Dicarbonyl Yields from the NOx-Air Photooxidations of a Series of Aromatic-Hydrocarbons in Air. *Environ. Sci. Technol.* **1986**, *20*, 383-387.

(4) Tuazon, E. C.; Atkinson, R.; Macleod, H.; Biermann, H. W.; Winer, A. M.; Carter, W. P. L.; Pitts, J. N. Yields of Glyoxal and Methylglyoxal from the NOx-Air Photooxidations of Toluene and m-Xylene and p-Xylene. *Environ. Sci. Technol.* **1984**, *18*, 981-984.

(5) Glowacki, D. R.; Lockhart, J.; Blitz, M. A.; Klippenstein, S. J.; Pilling, M. J.; Robertson, S. H.; Seakins, P. W. Interception of Excited Vibrational Quantum States by O_2 in Atmospheric Association Reactions. *Science (Washington, D. C., 1883-)* **2012**, *337*, 1066-1067.

(6) Hatakeyama, S.; Washida, N.; Akimoto, H. Rate Constants and Mechanism for the Reaction of OH (OD) Radicals with Acetylene, Propyne and 2-Butyne in Air at 297 K. *J. Phys. Chem.* **1986**, *90*, 173-178.

(7) Schmidt, V.; Zhu, G. Y.; Becker, K. H.; Fink, E. H. Study of OH Reactions at High Pressures by Excimer Laser Photolysis, Dye Laser Fluorescence. *Ber. Bunsen-Ges. Phys. Chem. Chem. Phys.* **1985**, *89*, 321-322.

(8) Hastings, W. P.; Koehler, C. A.; Bailey, E. L.; De Haan, D. O. Secondary Organic Aerosol Formation by Glyoxal Hydration and Oligomer Formation: Humidity Effects and Equilibrium Shifts During Analysis. *Environ. Sci. Technol.* **2005**, *39*, 8728-8735.

(9) Kroll, J. H.; Ng, N. L.; Murphy, S. M.; Varutbangkul, V.; Flagan, R. C.; Seinfeld, J. H. Chamber Studies of Secondary Organic Aerosol Growth by Reactive Uptake of Simple Carbonyl Compounds. *Journal of Geophysical Research-Atmospheres* **2005**, *110*.

(10) Liggio, J.; Li, S. M.; McLaren, R. Reactive Uptake of Glyoxal by Particulate Matter. *Journal of Geophysical Research-Atmospheres* **2005**, *110*, 13.

(11) Wittrock, F.; Richter, A.; Oetjen, H.; Burrows, J. P.; Kanakidou, M.; Myriokefalitakis, S.; Volkamer, R.; Beirle, S.; Platt, U.; Wagner, T. Simultaneous Global Observations of Glyoxal and Formaldehyde from Space. *Geophys. Res. Lett.* **2006**, *33*.

(12) Volkamer, R.; Molina, L. T.; Molina, M. J.; Shirley, T.; Brune, W. H. DOAS Measurement of Glyoxal as an Indicator for Fast VOC Chemistry in Urban Air. *Geophys. Res. Lett.* **2005**, *32*, 4.

(13) Salter, R. J.; Blitz, M. A.; Heard, D. E.; Kovacs, T.; Pilling, M. J.; Rickard, A. R.; Seakins, P. W. Quantum Yields for the Photolysis of Glyoxal Below 350 nm and Parameterisations for Its Photolysis Rate in the Troposphere. *Phys. Chem. Chem. Phys.* **2013**, *15*, 4984-4994.

(14) Salter, R. J.; Blitz, M. A.; Heard, D. E.; Pilling, M. J.; Seakins, P. W. A New Chemical Source of the HCO Radical Following Photoexcitation of Glyoxal, $(HCO)_2$. *J. Phys. Chem. A* **2009**, *113*, 8278.

(15) Salter, R. J.; Blitz, M. A.; Heard, D. E.; Pilling, M. J.; Seakins, P. W. Pressure and Temperature Dependent Photolysis of Glyoxal in the 355-414 nm Region: Evidence for Dissociation from Multiple States. *Phys. Chem. Chem. Phys.* **2013**, *15*, 6516-6526.

(16) Feierabend, K. J.; Flad, J. E.; Brown, S. S.; Burkholder, J. B. HCO Quantum Yields in the Photolysis of $(HCO)_2$ (Glyoxal) between 290 and 420 nm. *J. Phys. Chem. A* **2009**, *113*, 7784-7794.

(17) Feierabend, K. J.; Zhu, L.; Talukdar, R. K.; Burkholder, J. B. Rate Coefficients for the OH+Glyoxal Reaction between 210 and 390 K. *J. Phys. Chem. A* **2008**, *112*, 73-82.

(18) Fu, T. M.; Jacob, D. J.; Wittrock, F.; Burrows, J. P.; Vrekoussis, M.; Henze, D. K. Global Budgets of Atmospheric Glyoxal and Methylglyoxal, and Implications for Formation of Secondary Organic Aerosols. *Journal of Geophysical Research-Atmospheres* **2008**, *113*, 17-34.

(19) Niki, H.; Maker, P. D.; Savage, C. M.; Breitenbach, L. P. An FTIR Study of the Cl-Atom-Initiated Reaction of Glyoxal. *Int. J. Chem. Kinet.* **1985**, *17*, 547-558.

(20) Orlando, J. J.; Tyndall, G. S. The Atmospheric Chemistry of the HC(O)CO Radical. *Int. J. Chem. Kinet.* **2001**, *33*, 149-156.

(21) da Silva, G. Hydroxyl Radical Regeneration in the Photochemical Oxidation of Glyoxal: Kinetics and Mechanism of the HC(O)CO + O_2 Reaction. *Phys. Chem. Chem. Phys.* **2010**, *12*, 6698-6705.

(22) Setokuchi, O. Trajectory Calculations of OH Radical- and Cl Atom-Initiated Reaction of Glyoxal: Atmospheric Chemistry of the HC(O)CO Radical. *Phys. Chem. Chem. Phys.* **2011**, *13*, 6296-6304.

(23) Carslaw, N.; Creasey, D. J.; Harrison, D.; Heard, D. E.; Hunter, M. C.; Jacobs, P. J.; Jenkin, M. E.; Lee, J. D.; Lewis, A. C.; Pilling, M. J.et al. OH and HO_2 Radical Chemistry in a Forested Region of North-Western Greece. *Atmos. Environ.* **2001**, *35*, 4725-4737.

(24) Ren, X.; Olson, J. R.; Crawford, J. H.; Brune, W. H.; Mao, J.; Long, R. B.; Chen, Z.; Chen, G.; Avery, M. A.; Sachse, G. W.et al. HOx Chemistry During Intex-a 2004: Observation, Model Calculation, and Comparison with Previous Studies. *Journal of Geophysical Research-Atmospheres* **2008**, *113*.

(25) Pugh, T. A. M.; MacKenzie, A. R.; Hewitt, C. N.; Langford, B.; Edwards, P. M.; Furneaux, K. L.; Heard, D. E.; Hopkins, J. R.; Jones, C. E.; Karunaharan, A.et al. Simulating Atmospheric Composition over a South-East Asian Tropical Rainforest: Performance of a Chemistry Box Model. *Atmos. Chem. Phys.* **2010**, *10*, 279-298.

(26) Whalley, L. K.; Edwards, P. M.; Furneaux, K. L.; Goddard, A.; Ingham, T.; Evans, M. J.; Stone, D.; Hopkins, J. R.; Jones, C. E.; Karunaharan, A.et al. Quantifying the Magnitude of a Missing Hydroxyl Radical Source in a Tropical Rainforest. *Atmos. Chem. Phys.* **2011**, *11*, 7223-7233.

(27) MacDonald, S. M.; Oetjen, H.; Mahajan, A. S.; Whalley, L. K.; Edwards, P. M.; Heard, D. E.; Jones, C. E.; Plane, J. M. C. DOAS Measurements of Formaldehyde and Glyoxal above a South-East Asian Tropical Rainforest. *Atmos. Chem. Phys.* **2012**, *12*, 5949-5962.

(28) Peeters, J.; Nguyen, T. L.; Vereecken, L. HOx Radical Regeneration in the Oxidation of Isoprene. *Phys. Chem. Chem. Phys.* **2009**, *11*, 5935-5939.

(29) Taraborrelli, D.; Lawrence, M. G.; Crowley, J. N.; Dillon, T. J.; Gromov, S.; Gross, C. B. M.; Vereecken, L.; Lelieveld, J. Hydroxyl Radical Buffered by Isoprene Oxidation over Tropical Forests. *Nat. Geosci.* **2012**, *5*, 190-193.

(30) Wolfe, G. M.; Crounse, J. D.; Parrish, J. D.; St Clair, J. M.; Beaver, M. R.; Paulot, F.; Yoon, T. P.; Wennberg, P. O.; Keutsch, F. N. Photolysis, OH Reactivity and Ozone Reactivity of a Proxy for Isoprene-Derived Hydroperoxyenals (HPALDs). *Phys. Chem. Chem. Phys.* **2012**, *14*, 7276-7286.

(31) Fuchs, H.; Bohn, B.; Hofzumahaus, A.; Holland, F.; Lu, K. D.; Nehr, S.; Rohrer, F.; Wahner, A. Detection of HO_2 by Laser-Induced Fluorescence: Calibration and Interferences from RO_2 Radicals. *Atmos. Meas. Tech.* **2011**, *4*, 1209-1225.

(32) Stone, D.; Whalley, L. K.; Heard, D. E. Tropospheric OH and HO_2 Radicals: Field Measurements and Model Comparisons. *Chem. Soc. Rev.* **2012**, *41*, 6348-6404.

(33) Baeza Romero, M. T.; Blitz, M. A.; Heard, D. E.; Pilling, M. J.; Price, B.; Seakins, P. W.; Wang, L. Photolysis of Methylethyl, Diethyl and Methylvinyl Ketones and Their Role in the Atmospheric HOx Budget. *Faraday Discuss.* **2005**, *130*, 79-87.

(34) Baeza-Romero, M. T.; Glowacki, D. R.; Blitz, M. A.; Heard, D. E.; Pilling, M. J.; Rickard, A. R.; Seakins, P. W. A Combined Experimental and Theoretical Study of the Reaction between Methylglyoxal and OH/OD Radical: OH Regeneration. *Phys. Chem. Chem. Phys.* **2007**, *9*, 4114-4128.

(35) Carr, S. A.; Blitz, M. A.; Seakins, P. W. Site-Specific Rate Coefficients for Reaction of OH with Ethanol from 298 to 900 K. *J. Phys. Chem. A* **2011**, *115*, 3335-3345.

(36) Carr, S. A.; Glowacki, D. R.; Liang, C. H.; Baeza-Romero, M. T.; Blitz, M. A.; Pilling, M. J.; Seakins, P. W. Experimental and Modeling Studies of the Pressure and Temperature Dependences of the Kinetics and the OH Yields in the Acetyl + O_2 Reaction. *J. Phys. Chem. A* **2011**, *115*, 1069-1085.

(37) Lockhart, J.; Blitz, M. A.; Heard, D. E.; Seakins, P. W.; Shannon, R. J. Mechanism of the Reaction of OH with Alkynes in the Presence of Oxygen. *J. Phys. Chem. A* **2013**, *117*, 5407-5418.

(38) Plum, C. N.; Sanhueza, E.; Atkinson, R.; Carter, W. P. L.; Pitts, J. N. OH Radical Rate Constants and Photolysis Rates of Alpha-Dicarbonyls. *Environ. Sci. Technol.* **1983**, *17*, 479-484.

(39) Ghosh, B.; Papanastasiou, D. K.; Burkholder, J. B. Oxalyl Chloride, Clc(O)C(O)Cl: UV/Vis Spectrum and Cl Atom Photolysis Quantum Yields at 193, 248, and 351 nm. *J. Chem. Phys.* **2012**, *137*.

(40) Ianni, J. C. Kintecus, Windows Version 2.80, www.Kintecus.Com, 2002.

(41) Holbrook, K. A.; Pilling, M. J.; Robertson, S. H. *Unimolecular Reactions*, 2nd ed.; Wiley: Chichester, 1996.

(42) Pilling, M. J.; Smith, I. W. M. *Modern Gas Kinetics: Theory, Experiment and Application*; Blackwell Scientfic Publications: Oxford, 1987.

(43) Baeza Romero, M. T.; Blitz, M. A.; Heard, D. E.; Pilling, M. J.; Price, B.; Seakins, P. W. OH Formation from the $C_2H_5CO + O_2$ Reaction: An Experimental Marker for the Propionyl Radical. *Chem. Phys. Lett.* **2005**, *408*, 232-236.

(44) Siese, M.; Zetzsch, C. Addition of OH to Acetylene and Consecutive Reactions of the Adduct with O_2. *Z. Phys. Chemie-Int. J. Res. Phys. Chem. Chem. Phys.* **1995**, *188*, 75-89.

(45) DeSain, J. D.; Jusinski, L. E.; Ho, A. D.; Taatjes, C. A. Temperature Dependence and Deuterium Kinetic Isotope Effects in the $HCO(DCO)+O_2$ Reaction between 296 and 673 K. *Chem. Phys. Lett.* **2001**, *347*, 79-86.

(46) Glowacki, D. R.; Liang, C. H.; Morley, C.; Pilling, M. J.; Robertson, S. H. Mesmer: An Open-Source Master Equation Solver for Multi-Energy Well Reactions. *J. Phys. Chem. A* **2012**, *116*, 9545-9560.

(47) Frisch, M. J.; Trucks, G. W.; Schlegel, H. B.; Scuseria, G. E.; Robb, M. A.; Cheeseman, J. R.; Scalmani, G.; Barone, V.; Mennucci, B.; Petersson, G. A.et al. "Gaussian 09, Revision **A.1**," Gaussian, Inc., Wallingford CT, 2009.

(48) Mereau, R.; Rayez, M. T.; Rayez, J. C.; Caralp, F.; Lesclaux, R. Theoretical Study on the Atmospheric Fate of Carbonyl Radicals: Kinetics of Decomposition Reactions. *Phys. Chem. Chem. Phys.* **2001**, *3*, 4712-4717.

(49) Jagiella, S.; Zabel, F. Thermal Stability of Carbonyl Radicals - Part II. Reactions of Methylglyoxyl and Methylglyoxylperoxy Radicals at 1 Bar in the Temperature Range 275-311 K. *Phys. Chem. Chem. Phys.* **2008**, *10*, 1799-1808.

(50) Blitz, M. A.; Heard, D. E.; Pilling, M. J. OH Formation from CH_3CO+O_2: A Convenient Experimental Marker for the Acetyl Radical. *Chem. Phys. Lett.* **2002**, *365*, 374-379.

(51) Saunders, S. M.; Jenkin, M. E.; Derwent, R. G.; Pilling, M. J. Protocol for the Development of the Master Chemical Mechanism, MCM V3 (Part a): Tropospheric Degradation of Non-Aromatic Volatile Organic Compounds. *Atmos. Chem. Phys.* **2003**, *3*, 161-180.

(52) Dillon, T. J.; Crowley, J. N. Direct Detection of OH Formation in the Reactions of HO_2 with $CH_3C(O)O_2$ and Other Substituted Peroxy Radicals. *Atmos. Chem. Phys.* **2008**, *8*, 4877-4889.

(53) Hasson, A. S.; Tyndall, G. S.; Orlando, J. J. A Product Yield Study of the Reaction of HO_2 Radicals with Ethyl Peroxy, Acetyl Peroxy and Acetonyl Peroxy Radicals. *J. Phys. Chem. A* **2004**, *108*, 5979-5989.